Journal of Polymer Research (2019) 26: 222
https://doi.org/10.1007/s10965-019-1890-6

ORIGINAL PAPER

Using water to control electrospun Polycaprolactone fibre morphology for soft tissue engineering

Susana Gomes[1] · Diana Querido[1] · José Luís Ferreira[1,2] · João Paulo Borges[2,3] · Célia Henriques[1,2] · Jorge Carvalho Silva[1,2]

Received: 23 January 2019 / Accepted: 17 August 2019 / Published online: 21 August 2019

Abstract

Control of the properties of electrospun polycaprolactone can be achieved by adjusting the acetic acid:water ratio used to dissolve and electrospin the polymer. In this work, we studied the effect of using up to 15 wt% water in the solvent mixture. Solution conductivity and viscosity and fibre morphology vary dramatically with water content and solution age. Two days after initial solution preparation, electrospinning yields regular fibres for a water content of 0 wt% and 5 wt%, irregular fibres for a 10 wt% water content and irregular and fused fibres for a 15 wt% water content. Fibres with the highest crystallinity (60%) were obtained from solutions containing 5 wt% water while the highest elastic modulus (8.6 ± 1.4 MPa) and tensile stress (4.3 ± 0.3 MPa) pertain to fibres obtained from solutions containing 10 wt% water. Enzymatic fibre degradation is faster the higher the water content in the precursor solution. Adhesion ratio of human foetal fibroblasts was highest on scaffolds obtained from precursor solutions containing 0 wt% water. Cell population increases for all scaffolds and populations quickly become equivalent, with no statistically significant differences between them. Cells exhibit a more extended morphology on the 5 wt% scaffold and a more compact morphology on the 0 wt% scaffold. In summary, a small water content in the solvent allows a significant control over fibre diameter, scaffold properties and the production of scaffolds that support cell adhesion and proliferation. This strategy can be used in soft tissue engineering to influence cell behaviour and the degradation rate of the scaffolds.

Keywords Electrospinning · Polycaprolactone · Acetic acid:Water solvent mixture · Fibre morphology · Cell adhesion · Tissue engineering

Introduction

Electrospinning is a simple and efficient technique for the fabrication of polymeric fibres, ranging in diameter from a few microns down to tens of nanometres [1]. These structures have gained importance in the field of tissue engineering as biodegradable scaffolds mainly because of their high surface to volume ratio, high porosity and resemblance with the morphology of the native extracellular matrix [2, 3]. The scaffold's morphology and the chemical nature of the constituent materials are two factors affecting the overall physical and chemical properties of the scaffold and the way cells interact with it during adhesion, migration and differentiation, which are important processes in tissue regeneration [4, 5]. Scaffolds with different mechanical properties are required for the regeneration of different tissues such as bone, cartilage, blood vessels, nerves and tendons. The ability to process materials of natural and synthetic origin by electrospinning has been exploited to achieve such particular requirements [6, 7].

Among the various biodegradable materials available, polycaprolactone (PCL), a semi-crystalline poly(α-hydroxy ester), presents excellent biocompatibility, low cost, acceptable degradation kinetics and good mechanical properties for many biological applications [8–14]. Electrospun PCL fibres are widely known for their potential in biomedical and tissue engineering applications, being able to support adhesion,

✉ Jorge Carvalho Silva
jcs@fct.unl.pt

[1] Physics Department, Faculty of Science and Technology, Universidade NOVA de Lisboa, Campus de Caparica, 2829-516 Caparica, Portugal

[2] CENIMAT/I3N, Faculty of Science and Technology, Universidade NOVA de Lisboa, Campus da Caparica, 2829-516 Caparica, Portugal

[3] Materials Science Department, Faculty of Science and Technology, Universidade NOVA de Lisboa, Campus da Caparica, 2829-516 Caparica, Portugal

proliferation and differentiation of stem cells [15, 16]. Due to PCL's hydrophobic nature and the absence of enzymes capable of efficiently degrading it in vivo, degradation of bulk PCL in vivo is a slow process that lasts years and begins with chain scission by hydrolytic cleavage of ester groups [17]. When the particle size of the implant decreases due to fragmentation or when powdered samples are implanted, PCL is rapidly degraded in a few days inside the phagosomes of macrophages and giant cells [18]. Therefore, the characteristic size of implanted scaffolds plays a critical role on their degradation rate and fibre diameter can be used to control the permanence time of electrospun scaffolds in vivo.

The structure of electrospun mats depends on several variables, including polymeric solution properties (viscosity, surface tension and conductivity), process parameters (applied voltage, flow rate, tip to collector distance), and environmental conditions (temperature, humidity) [19]. There are different solvent systems reported for the dissolution of PCL that have a direct effect on the properties of fibre mats electrospun from the corresponding solutions [20–24]. Among these solvents, acetic acid may be the most convenient when a blend of PCL with hydrophilic polymers, such as chitosan, is to be achieved [25, 26]. However, there is a lack of information relating the effect of using acetic acid as a pure solvent or mixed with water on the morphology, crystallinity and mechanical properties of nonwoven PCL fibres, despite their importance in defining the properties of an engineered scaffold. The mechanical properties of polymers are strongly influenced by the molecular orientation and crystallinity of electrospun fibres and play an important role in stem cell differentiation [27]. Crystalline domains in electrospun PCL micro- and nanofibres have been shown to assume a plate-like lamellar shape oriented more or less perpendicularly to the long fibre axis [28].

In order to understand the effect of dissolving PCL in mixtures of acetic acid with water on the outcome of the electrospinning process and on the properties of the resulting fibre mats, in this work we prepared four PCL solutions using solvents with different acetic acid:water ratios. Recently, Li et al. [24] performed an optimization of the system PCL dissolved in acetic acid and water and studied fibre diameter and crystallinity from XRD diffractograms. Ultrafine PCL nanofibers with average diameters around 200 nm were produced using a water concentration of 9 vol% and a PCL concentration in the range 17% to 20%. Here, we extend the work of Li et al. [24] by determining additional properties of the fibre mats: physical (thermal and mechanical properties), chemical (enzymatic degradation tests) and biological (cell adhesion, proliferation and morphology). The concentration of PCL was fixed at 23%, based on our previous study of PCL electrospinning using glacial acetic acid as solvent [23], and the water content in the solvent varied from 0% to 15%. These solutions were successfully electrospun and the resulting fibre mats were then characterized using: scanning electron microscopy (SEM) to observe fibre morphology and arrangement and to obtain the fibre diameter distribution; differential scanning calorimetry (DSC) to determine the melting temperature and enthalpy as well as the crystallinity; tensile tests to obtain the elastic modulus; and degradation studies with microbial lipase to assess and compare the susceptibility of scaffolds to enzymatic degradation if implanted in vivo. Finally, an in vitro study was performed to relate those properties with potential differences in adhesion, proliferation and morphology of cells seeded on these scaffolds.

Materials and methods

Polymeric solutions

The solutions were made with PCL (Mn 80 kg·mol^{-1}) from Sigma-Aldrich and glacial acetic acid (purity 99.8%) from Pronolab. All materials were used as received.

Four different solutions were prepared, all with a polymer concentration of 23 wt%, in glass flasks with air-tight lids. The solvents were prepared by mixing glacial acetic acid with distilled water with the mass ratios 100:0, 95:5, 90:10 and 85:15. PCL would no longer dissolve when the water content was further increased to 20 wt%. As a general rule, solutions were magnetically stirred for about 48 h and placed in an ultrasound bath for 10 min to achieve complete dissolution of PCL. For the analysis of solution properties and fibre morphology as a function of time elapsed since initial solution preparation, solutions were kept in the magnetic stirrer for 4, 9 and 13 days.

Surface tension was measured using the pendant drop method in a CAM101 tensiometer from KSV. Electrical conductivity was measured using a conductivity meter HI 4521 model from Hanna Instruments. Shear viscosity was measured at 25 °C using a Bohlin Gemini HRnano rotational rheometer from Malvern Instruments equipped with 40 mm, 2°, cone and plate fixtures.

Electrospinning

PCL fibre mats were obtained by electrospinning the four solutions. The electrospinning apparatus was set up horizontally and a grounded 20 cm × 20 cm aluminium plate covered with aluminium foil was used to collect the fibres. The collector had translational and rotational movements in its plane in order to achieve the production of fibre mats with a more uniform thickness. A syringe pump (New Era Pump Systems) was used to control the polymer solution flow rate and a high voltage DC power supply (Iseg) was used to charge the solution and create the electric field between the needle and the collector. All solutions were electrospun at a room temperature between 22 °C and 24 °C and a relative humidity

between 40% and of 50% using the following parameters: a high voltage of 8.0 kV, a needle-collector distance of 10 cm and a feed rate of 0.3 ml·h^{-1}. The solution was ejected from a blunt stainless-steal needle (23G).

Fibre mat characterization

The electrospun fibre mat's morphology was analyzed by scanning electron microscopy (SEM). Samples were mounted on stubs using a double-side conductive tape and sputter coated with gold before SEM observation. The SEM images were acquired with a Zeiss DSM 902 Scanning Electron Microscope operating in high vacuum at 5 kV with different magnifications.

The melting point and the melting enthalpy of each fibre mat were measured using a SETARAM-DSC92 differential scanning calorimeter. The samples were heated at a rate of 10 °C·min^{-1} under a nitrogen atmosphere from −30 °C up to 100 °C. The crystallinity of the fibres was then estimated from the ratio between the melting enthalpy of each fibre mat and the melting enthalpy of the 100% crystalline PCL, which has an estimated value of 139.5 J·g^{-1} [29].

Mechanical properties of the four different fibre mats were measured with a uniaxial tensile testing machine from Rheometric Scientific equipped with a 20 N load cell. Ten replicas from two mats obtained with each solvent were tested at a speed of 5 mm·s^{-1}. Rectangular samples were cut with a surface area of 10 mm × 30 mm and mounted on the testing machine such that the pulled length was 10 mm. Thickness of the samples was measured using a digital micrometer (Mitutoyo, Japan).

Enzymatic degradation tests were performed using an esterase, Lipase PS "Amano" SD, a generous gift of Amano Enzyme Europe. This lipase is produced by a selected strain of *Burkholderia cepacia* and has an activity (FIP method) of not less than 23,000 U/g. Samples were cut with an approximately square shape from at least two different depositions and placed in glass vials. Triplicates with roughly the same mass were prepared for each of the four fibre mats. Lipase was dissolved in distilled water at a concentration of 1 mg/ml. To each vial, 2 ml lipase solution were added. The vials were first placed in a vacuum desiccator in order to remove air from the mat's interior and then placed in an incubator at 37 °C under mild orbital rotation. After a total of 1, 2, 4, 6 and 9 h, the lipase solution was removed, the samples were washed with distilled water, dried in an oven at 37 °C and weighed. The degradation tests were performed a total of 4 times.

Experimental values for average fibre diameter and Young's modulus are presented as mean ± experimental standard deviation. The crystallinity values are presented as value ± standard combined uncertainty. Results of the degradation tests are presented as mean ± standard deviation of the mean. Statistical significance of the differences between results was evaluated using Student's *t* test.

Cell seeding and culture

Five samples of each mat were sterilized by immersion in ethanol 70% for 10 min and then washed twice with sterile PBS to remove ethanol. Fibres were then irradiated with UV light for 30 min, transferred to individual teflon inserts that delimit an 8 mm diameter seeding surface and placed in a 24-well tissue culture plate.

HFFF2 cells (Human Foetal Foreskin Fibroblast cells, acquired from the European Collection of Cell Cultures, UK) were cultured with DMEM + GlutaMAX, supplemented with Fetal Bovine Serum (10% *v*/v), penicillin G (100 units·mL^{-1}) and streptomycin (100 μg·mL^{-1}), all from Invitrogen, and maintained at 37 °C in a 5% CO_2 humidified atmosphere. Cells in their passage 9 were seeded in 25 cm^3 T-flasks. While sub-confluent, cells were detached using Tryple (Invitrogen), counted and seeded over the fibre mats at a density of 2×10^4 cells·cm^{-2}. Control wells were set by seeding cells directly on the polystyrene tissue culture plates using the same seeding density.

Cell adhesion, proliferation and morphology

Adhesion and proliferation of cells seeded on the mats were evaluated using the resazurin cell viability assay. The cell population was monitored 1, 3, 5, and 7 days after cell seeding. Cultures were inspected during the experiment under an inverted light phase contrast microscope (Nikon Eclipse Ti-S) to confirm cell growth in the controls and sterility.

For the resazurin assay, the medium of each well was removed and replaced by a mixture of 200 μL of fresh culture medium and 10% (*v*/v) resazurin reagent solution. After incubating cells for 2 h, a fixed volume of cell supernatant was transferred from each insert to a 96-well plate and the optical density was read at 570 nm and 600 nm in a plate reader (BioTek ELX800UV). Appropriate medium controls – wells containing only culture medium and the resazurin solution - were also set up.

Cell adhesion was obtained by comparing the absorbance of the supernatant of cells cultured on the fibre mats to that of the cell control 24 h after cell seeding. Cell adhesion assays were performed in triplicate and the results presented as (mean ± experimental standard deviation).

Cell culture proceeded in order to evaluate cell proliferation following a procedure similar to that used for cell adhesion determination, measuring the absorbance of the supernatant of cultured cells on the fibre mats every two subsequent days. The results are expressed as mean ± experimental standard deviation.

Student's *t* test was used to evaluate significance of the differences between cell adhesion rates and cell populations on the last day (day 7) on the 4 scaffolds under analysis.

To evaluate cell morphology, HFFF2 cells were seeded on the fibre mats as previously described. After 2 and 10 days of culture, the samples were fixed with 3.7% paraformaldehyde in PBS at room temperature for 15 min. Then, samples were rinsed twice with PBS and stained with Acti-stain 555 Fluorescent Phalloidin from Cytoskeleton, Inc., for the fluorescent visualization of actin filaments and counterstained with DAPI for nuclei visualization. Cells were then imaged using a Nikon Eclipse Ti-S microscope with epifluorescence attachment. Images were acquired with a Nikon D610 camera and processed using the ImageJ software [30]. Where necessary, contrast and brightness of the original images were minimally adjusted within the linear range to improve visual clarity.

Results and discussion

Solution properties

The properties of the four PCL solutions are listed in Table 1 as a function of solution age (days elapsed since initial preparation). Solution properties were measured on days 2 and 4 and, for the 100:0 solution, on days 9 and 13 as well.

The surface tension of all solutions was found to be around 32 $mN{\cdot}m^{-1}$, irrespective of the water content in the solvent and solution age and roughly 5 $mN{\cdot}m^{-1}$ above the surface tension of glacial acetic acid (27.12 $mN{\cdot}m^{-1}$, at 25 °C) [31]. Álvarez et al found that the surface tension of organic acid:water mixtures varies slowly when the concentration of the organic acid is high: for acetic acid, the surface tension at 25 °C increased by only 25% (6.7 $mN{\cdot}m^{-1}$) when the molar fraction of water went from 0% to 59% [31]. In our case, a constant surface tension implies that the different outputs of the electrospinning process are not caused by a variation of the solution's surface tension but rather by changes in viscosity and conductivity.

The conductivity of the solutions increased by two orders of magnitude when the water content changed from 0% to a mere 15%. The conductivity of the 100:0 solution is very small due to the low degree of ionization of acetic acid caused by the near absence of water molecules in the solution. When the concentration of water increases, the increased availability of proton acceptors leads to a significant ionization of acetic acid and a concomitant increase of charge carriers and therefore of conductivity. A higher conductivity facilitates the stretching of the polymer jet during electrospinning due to the increased number of charges transported and repulsion forces between these [32]. The conductivity didn't show any dependence on time elapsed since solution preparation.

The viscosity of the solutions decreases drastically with both water content and solution age. This fact has important consequences regarding the ability to electrospin the solutions for a decreased viscosity facilitates the stretching of the polymer jet by the repulsive forces between the charges transported by the jet, leading to thinner fibres [19]. However, a low viscosity leads to a rapid and pronounced thinning of the jet, which may be detrimental to the uniformity of the electrospun fibres due to the increased influence of surface tension that causes the appearance of beaded fibres [24]. The decrease in solution viscosity with age is due to the degradation of PCL: the acid environment catalysis the hydrolytic degradation of ester linkages leading to a decrease in average molar mass and solution viscosity [33].

Fibre morphology

Figure 1 shows the morphology and arrangement of the electrospun fibres obtained from the 100:0, 95:5, 90:10 and 85:5 solutions, respectively, for different solution ages. Fibres

Table 1 Properties of solutions with 23 wt% PCL and different acetic acid:water mixtures as a function of solution age (days elapsed since initial preparation)

Acetic acid:water (wt% ratio)	Solution age t / days	Surface tension γ / ($mN\ m^{-1}$)	Conductivity σ / ($\mu S\ cm^{-1}$)	Zero shear viscosity η / (Pa s)
100:0	2	32.6 ± 0.5	0.057 ± 0.006	42 ± 4
	4	31.8 ± 0.7	0.059 ± 0.007	27 ± 4
	9	32.1 ± 0.5	0.063 ± 0.007	11 ± 1
	13	31.8 ± 0.4	0.061 ± 0.006	5.9 ± 0.8
95:5	2	32.6 ± 0.3	0.50 ± 0.05	4.6 ± 0.5
	4	32.5 ± 0.4	0.53 ± 0.06	2.9 ± 0.2
90:10	2	33.7 ± 0.4	1.9 ± 0.2	1.2 ± 0.2
	4	32.0 ± 0.3	2.0 ± 0.2	0.6 ± 0.1
85:15	2	33.5 ± 0.3	5.6 ± 0.6	0.5 ± 0.2
	4	32.0 ± 0.3	5.8 ± 0.6	0.24 ± 0.03

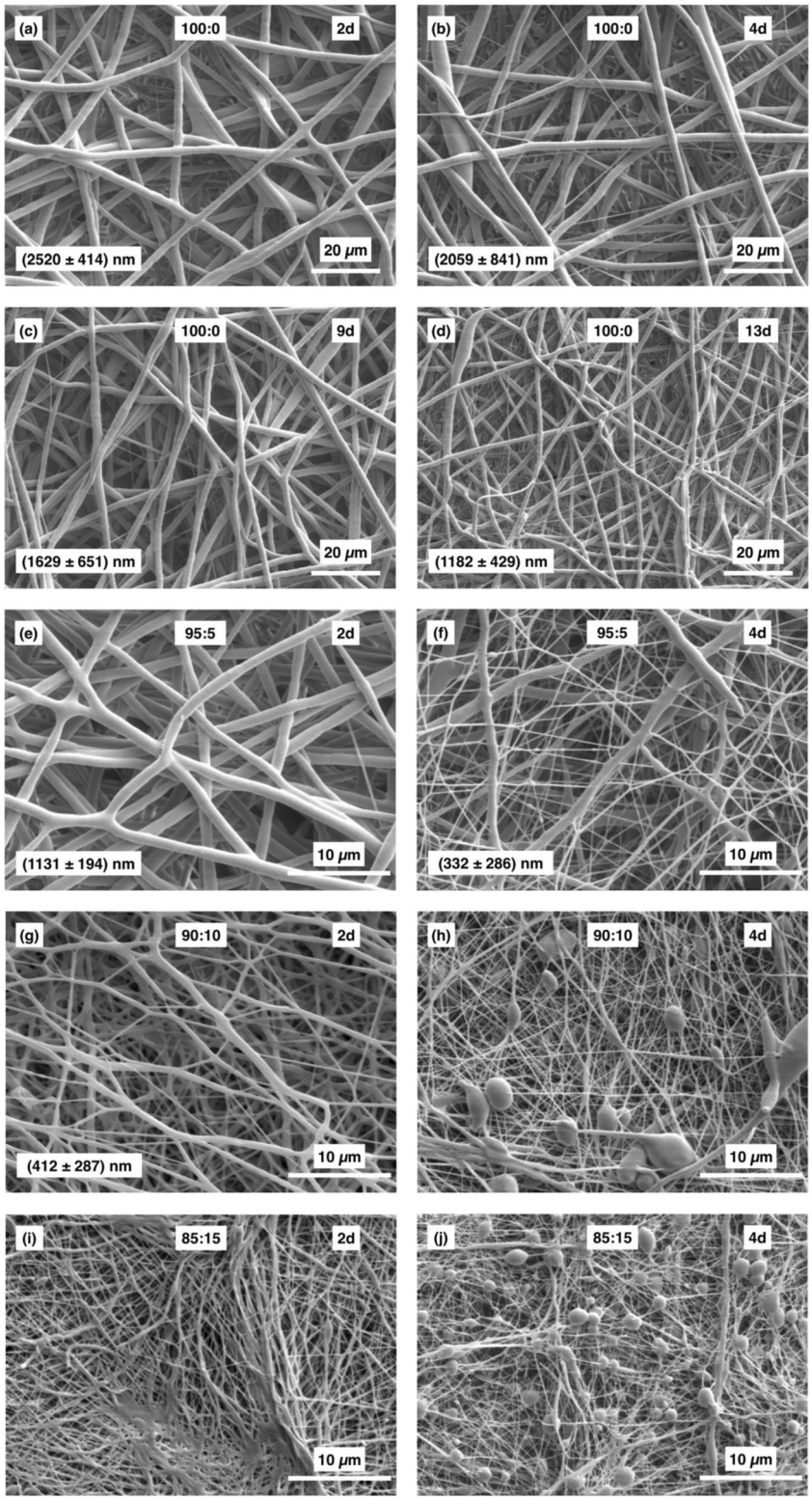

Fig. 1 Morphology of the PCL electrospun fibres obtained from the (**a**), (**b**), (**c**) and (**d**) 100:0 solution; (**e**) and (**f**) 95:5 solution; (**g**) and (**h**) 90:10 solution; (**i**) and (**j**) 85:15 solution. Days elapsed since initial solution preparation are indicated on the SEM images. Measurements are average fibre diameter ± standard deviation of fibre diameter distribution. Magnifications and scale bars are 1000X and 20 μm in images (**a**)-(**d**) and 3000X and 10 μm in images (**e**)-(**j**)

obtained from the 100:0 solutions 2 days after solution preparation (Fig. 1 (a)) are the thickest of all, with an average diameter of (2520 ± 414) nm. These values are similar to those reported by Kanani et al. for 20% PCL solutions in glacial acetic acid [34]. For PCL dissolved in chloroform, reported average diameters vary significantly, from 400 nm up to 8 μm, as a function of polymer concentration and processing conditions [8, 23, 35, 36]. As solution ages, the average fibre diameter decreases, reaching (1181 ± 429) nm 13 days after preparation. This decrease is due to the decrease in solution

viscosity, as previously discussed. After 13 days, the fibres began showing significant defects (images not shown).

The effect of water content on fibre morphology and diameter can be seen in Fig. 1 a), e), g) and i) that correspond to fibres obtained from solutions containing 0%, 5%, 10% and 15% water 2 days after solution preparation. Fibre diameter diminishes markedly, from (2520 ± 414) nm for the 0% water content to (1131 ± 194) nm for 5% water and (412 ± 287) nm for 10% water. Fibres obtained from the 85:15 solution are very thin but irregular and fused; as such, their diameter was not measured. As the water content in the precursor solutions increases, so does conductivity, whereas viscosity decreases. Both of these variations favour the rapid elongation and thinning of the polymer jet. Jet elongation causes a separation of the electrical charge transported by the jet and consequently the decrease of the repulsive forces between charges. If this repulsion relaxes before jet solidification, then surface tension may cause the appearance of beads, which correspond to local minima of the surface area to volume ratio, along the fibres [19].

For fibres obtained from the 95:5 solution 4 days after preparation (Fig. 1 f) the standard deviation of the fibre diameter distribution is large, denoting a somewhat unstable process, with the thinnest fibres having less than 100 nm diameter and the thickest fibres having around 1.2 μm diameter. Fibres obtained from the 90:10 and 85:15 solutions at 4 days of age (Fig. 1 h and j) display a large number of spherical beads.

Thermal properties

The DSC thermograms of the four PCL membranes are shown in Fig. 2 while the melting temperature, melting enthalpy and crystallinity are listed in Table 2. All membranes display a single endothermic peak in the interval [0; 100] °C. This peak, located around 64 °C, corresponds to the melting temperature of PCL [29]. The different peak shapes observed may be artefacts caused by different rates of heat transfer in the samples caused by their porous structure. The melting enthalpy is obtained from the area beneath the peaks. Values range from 67.1 J/g for the 100:0 membrane to 83.5 J/g for the 95:5 membrane. Accordingly, the crystallinity, calculated from the ratio between the melting enthalpy of each fibre mat and the melting enthalpy of the 100% crystalline PCL is the highest for the 95:5 membrane: 60%, versus 48% for the 100:0 membrane. The 90:10 and the 85:15 membranes have crystallinities in between: 52% and 49%, respectively.

For PCL dissolved in chloroform, Hsu and Shivkumar report crystallinities in the range 30–35%, for different processing conditions [37], whereas Lowery et al. obtained 47% [36]. For PCL dissolved in dimethylformamide:chloroform mixture, Wong et al. obtained crystallinities ranging from 42% to 50% as the dimethylformamide content increased [38]. The lower volatility of DMF led to the production of thinner and more crystalline fibres due to slower solvent evaporation which allowed for a greater thinning of the polymer jet and an increased arrangement of the polymer chains into crystalline domains. In Wong et al.'s work, thinner fibres are more

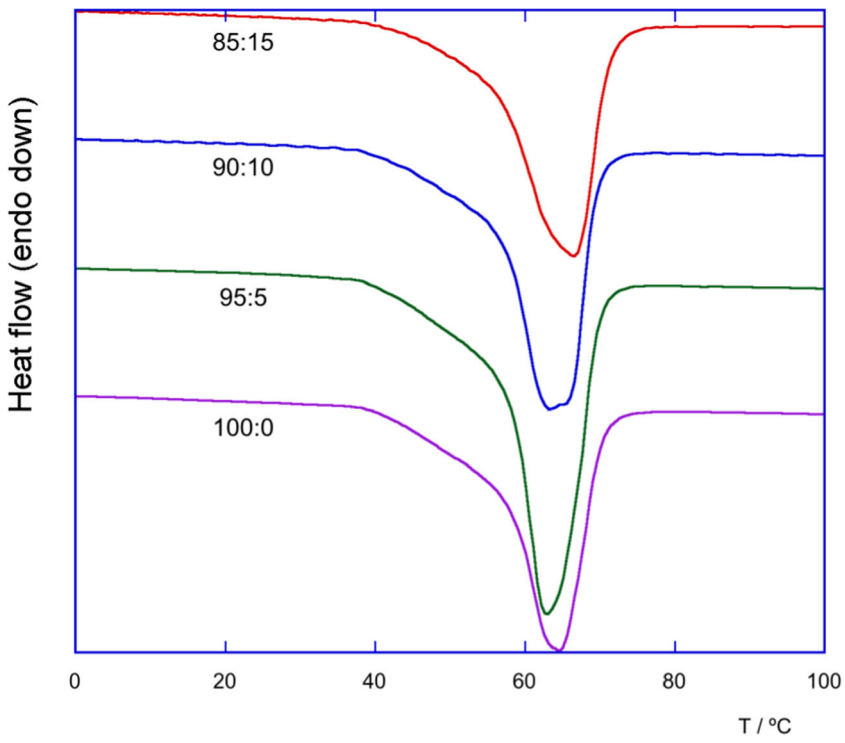

Fig. 2 DSC curves of PCL non-woven mats obtained using different acetic acid:water ratios

Table 2 DSC results for melting point, enthalpy and crystallinity of PCL fibre mats obtained from 23 wt% PCL solutions using different acetic acid:water mixtures

Acetic acid:water (wt% ratio)	Melting point T_m / °C	Melting enthalpy ΔH_m / (J·g^{-1})	Crystallinity $w_{c,x}$ / %
100:0	63.4	67.1	48
95:5	63.5	83.5	60
90:10	63.4	72.2	52
85:15	64.2	68.5	49

crystalline: the same trend was observed in our work. Fibres obtained from the 95:5 solution display the same morphology and arrangement as those obtained from the 100:0 solution but their average diameter is less than half. While fibres obtained from the 90:10 solution have an even smaller average diameter, their morphology is irregular, a feature that worsens for fibres obtained from the 85:15 solution. This suggests that fibre diameter is not the only factor affecting crystallinity but the addition of a small amount of a non-solvent like water may also be beneficial for crystalline domain development. However, as the water content in solution is further increased to 10 wt% and 15 wt%, fibre crystallinity decreases.

Mechanical properties

Values of elastic modulus of PCL non-wovens reported in the literature for PCL electrospun using different solvents and at different concentrations lie typically within the range 2 to 10 MPa [39, 40]. Mechanical properties of individual PCL fibres have also been reported in the literature. Tensile testing of individual PCL fibres yielded an elastic modulus of (120 ± 30) MPa for (1.4 ± 0.3) μm fibres when PCL was dissolved at a concentration of 7.5% using chloroform:methanol 3:1 as a solvent [41], and of 0.5 GPa for fibres with a diameter in the range 200 nm to 2500 nm electrospun from a 10 wt% PCL solution using a dichloromethane: N,N-dimethylformamide 4:1 solvent mixture [42]. Using a three-point bending method, Croisier et al. obtained a mean value of (3.7 ± 0.7) GPa for the Young's modulus of individual fibres obtained from a 15 wt% solution of PCL dissolved in 1:1 tetrahydrofurane/N,N-dimethylformamide [4]. The difference between the elastic modulus of non-woven mats and that of individual fibres can be explained by the high porosity and random orientation of the fibres in the non-woven mats.

The results of the tensile tests performed on the four types of membranes are displayed in Fig. 3 that shows typical stress-strain curves and in Table 3 that lists the elastic modulus, the tensile stress and the tensile strain obtained. In spite of the very different average fibre diameter, the 100:0 and 95:5 membranes display similar stress-strain curves that reveal a ductile behaviour. The similarity between the 100:0 and 95:5 membranes also shows up in the elastic modulus obtained: (4.7 ± 0.7) MPa and (5.4 ± 0.8) MPa, respectively. The 90:10 membrane has the highest elastic modulus: (8.6 ± 1.4) MPa. Since the 90:10 membrane is less crystalline than the 95:5 membrane, the higher elastic modulus may be due to differences in fibre morphology, diameter and bonding between fibres. The higher water content used in the preparation of the

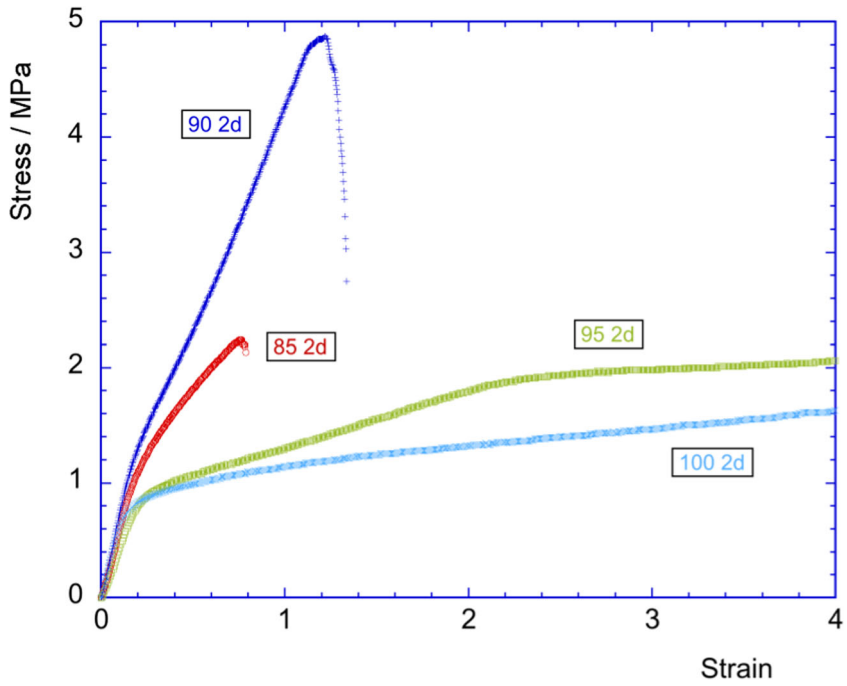

Fig. 3 Typical stress-strain curves of the four PCL fibre mats on day 2. The 100:0 and the 95:5 membranes display identical stress/strain behaviour. The 90:10 membrane has the highest tensile strength and the 85:15 the smallest tensile strain

Table 3 Mechanical properties of the PCL membranes obtained from 23 wt% PCL solutions using different acetic acid:water mixtures. Young's modulus (*E*), tensile stress (σ) and tensile strain (ε) for different times elapsed since initial solution preparation

Acetic acid:water (wt% ratio)	Day	Young's modulus *E* / MPa	Tensile stress σ / MPa	Tensile strain ε / %
100:0	2	4.7 ± 0.7	*	>500
	4	6.9 ± 1.4	*	>500
	9	5.2 ± 1.1	*	>500
	13	5.6 ± 1.1	*	>500
95:5	2	5.4 ± 0.8	*	>500
	4	4.3 ± 1.3	1.5 ± 0.2	80 ± 8
90:10	2	8.6 ± 1.4	4.3 ± 0.3	88 ± 5
	4	4.0 ± 0.8	1.8 ± 0.2	59 ± 4
85:15	2	6.5 ± 0.6	2.2 ± 0.2	73 ± 3

*Tensile stress and strain could not be determined since the membranes did not rupture during the test

90:10 membrane leads to a smaller evaporation rate of the solvent (the evaporation rate of water relative to butyl acetate is 0.3 while that of acetic acid is 0.97) which may lead to incomplete solvent evaporation when the fibres reach the collector and fibre bonding at their contact points. This phenomenon, which can be seen for the 90:10 membrane, is even more pronounced for the 85:15 membrane. While differences in fibre morphology between the 95:5 and the 90:10 membranes are not significant, fibre diameter is much smaller and diameter distribution much wider for the 90:10 membrane. Tensile testing of single electrospun PCL nanofibres revealed a significant increase in tensile modulus and strength as the diameter of individual electrospun PCL fibres decreased below 600–700 nm [38, 43, 44]. These results may explain why the 90:10 membrane, composed of fibres with diameters in the interval (412 ± 287) nm, possesses the highest elastic modulus of all 4 membranes.

Silver et al. determined that the elastic modulus of human skin and dermis for strains up to 0.4 is 0.10 MPa and that the modulus increases above a strain of 0.4 to 18.8 MPa [45]. Although the stress-strain curves of skin and of the mats produced in the current work are different, the range of elastic modulus reported for skin contains the values determined for our PCL non-woven mats, which suggests their mechanical behaviour is adequate for soft tissue engineering applications.

Degradation tests

Degradation tests were performed using lipase produced by *Burkholderia cepacia* that is known to catalyse the hydrolytic degradation of PCL [46, 47]. Chain scission causes a decrease of molecule mass, eventually leading to soluble oligomers. The concentration used in this study, 23,000 U/L, is about 200 times higher than that found in the serum of healthy adults [48]. This led to a total degradation of all mats in under 10 h. When implanted in vivo, PCL may take several years to degrade but micrometre-sized structures degrade in a few days [17, 18]. The results of the present degradation study are shown in Fig. 4 where the remaining scaffold's mass, relative to the initial mass, is plotted against time. The higher the water concentration in the precursor solutions of the fibre mats, the faster mass loss occurred. This is attributed to the degradation of PCL that occurred in solution before electrospinning commenced. Lowering of molecular mass caused by hydrolytic scission of ester bonds also caused a decrease of solution viscosity with increasing water content. These results show that the in vivo permanence of PCL electrospun scaffolds can be controlled through a preceding polymer degradation. This is equivalent to using different PCL molar masses in scaffold production.

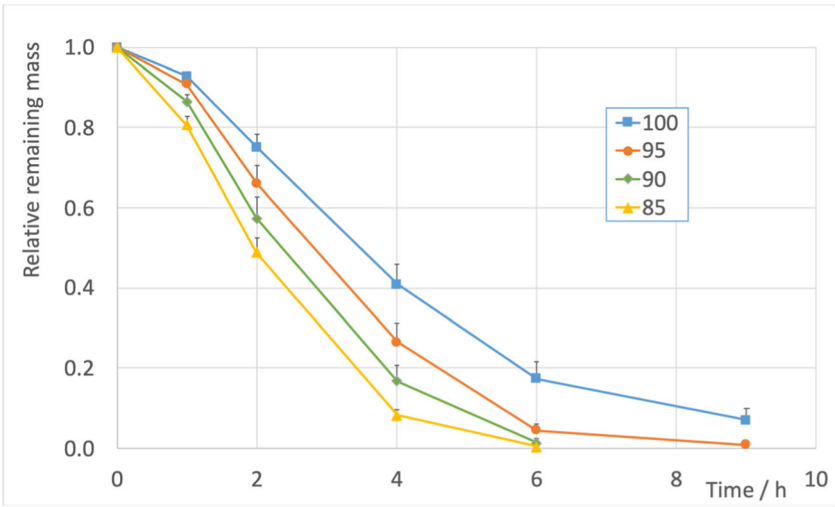

Fig. 4 Degradation of PCL scaffolds by lipase in accelerated conditions using a 1 mg/ml lipase concentration. Scaffolds obtained using solutions with a higher water concentration suffer a faster degradation as revealed by remaining mass measurements. This fact may be used to tune scaffold permanence when implanted in vivo

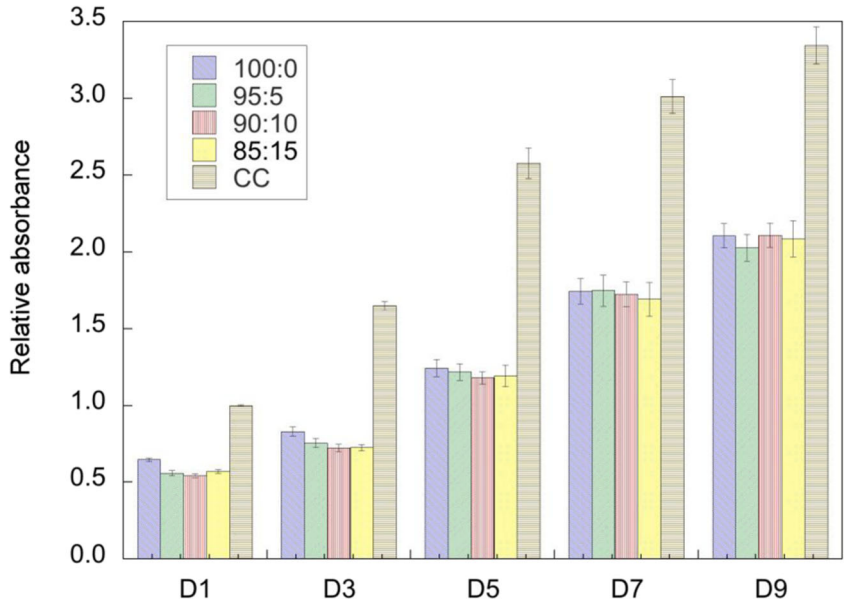

Fig. 5 Results of the resazurin viability assay performed on four time points after cell seeding. CC is cell control. All absorbances are normalized to day 1 CC value. Vertical bars represent the standard deviation of the mean

HFFF2 adhesion and proliferation

Figure 5 plots the absorbance values of the culture media to which resazurin was added, part of which was reduced into resorufin by the viable cells. All absorbances are normalized to the cell control (CC) day 1 results. The absorbance values measured on day 1 can be used to establish an adhesion efficacy by calculating the ratio between the values measured for the wells containing cells seeded on the PCL scaffolds and those obtained for the cell control, for which adhesion efficacy is assumed to be 100%. Table 4 presents the adhesion ratios and the statistical significance of the differences. The adhesion ratio is (65 ± 6) % for the 100:0 membrane, about 10% higher than for the remaining membranes, with the differences being all statistically significant. When comparing the adhesion ratios of the 95:5, 90:10 and 85:15 membranes, which lie in the interval 54% to 57%, the conclusion is that the differences are not statistically different.

As time progresses, cell populations increase and quickly become similar, with the differences between membranes losing statistical significance on day 5. This means that, independently of initial cell adhesion ratio and membrane morphology, HFFF2 cells are able to proliferate on and populate all scaffolds.

Table 4 Adhesion ratio of HFFF2 cells seeded on the four PCL scaffolds relative to the cell control and result of statistical significance test. Ratios calculated from absorbances measured 24h after seeding. Y=Yes ($p < 0.01$) and N=No ($p \geq 0.01$)

Scaffold	Adhesion ratio / %	CC	100:0	95:5	90:10	85:15
CC	100 ± 3	–	Y	Y	Y	Y
100:0	65 ± 6	<0.001	–	Y	Y	Y
95:5	56 ± 7	<0.001	<0.001	–	N	N
90:10	54 ± 6	<0.001	<0.001	0.321	–	N
85:15	57 ± 6	<0.001	<0.001	0.323	0.027	–

To evaluate cell morphology, cells were fixed 2 and 10 days after seeding and stained with fluorescent dyes for F-actin and nuclei (see Fig. 6). Two days after seeding, most cells exhibit an extended morphology that suggests the establishment of several adhesion contacts with the scaffold. Cells appear to adopt a more extended morphology on the 95:5 scaffold and a more compact morphology on the 100:0 scaffold. This difference seems to be related with fibre diameter suggesting an easier spreading of HFFF2 fibroblasts on PCL scaffolds having thinner fibres and that cells established adhesions with fewer fibres on the 100:0 scaffold. On day 10, cells are seen populating most of the scaffold's surface on all four cases but the more compact morphology of cells on the 100:0 scaffold seems to persist.

Cell adhesion to pure PCL scaffolds has been shown to occur at a reasonable level in comparison to controls and other polymers or PCL blends [7, 8, 49]. A partial explanation to this fact may be the enhanced protein adhesion to nanofibrous scaffolds that compensates for the hydrophobicity and lack of cell recognition sites of PCL [50]. Mean fibre diameter and fibre uniformity may also play an important role in modulating cell attachment and proliferation. As Chen et al. pointed out [51], fibroblast adhesion to PCL electrospun fibres with diameters in the range [117–1647] nm was lowest to the thinner and beaded fibres as we found in our study. Additionally, Washburn et al. concluded from an investigation of osteoblast response to different polymer crystallinities that cells are exquisitely sensitive to variations in nanometre-scale topography that results from variations in crystallinity [52].

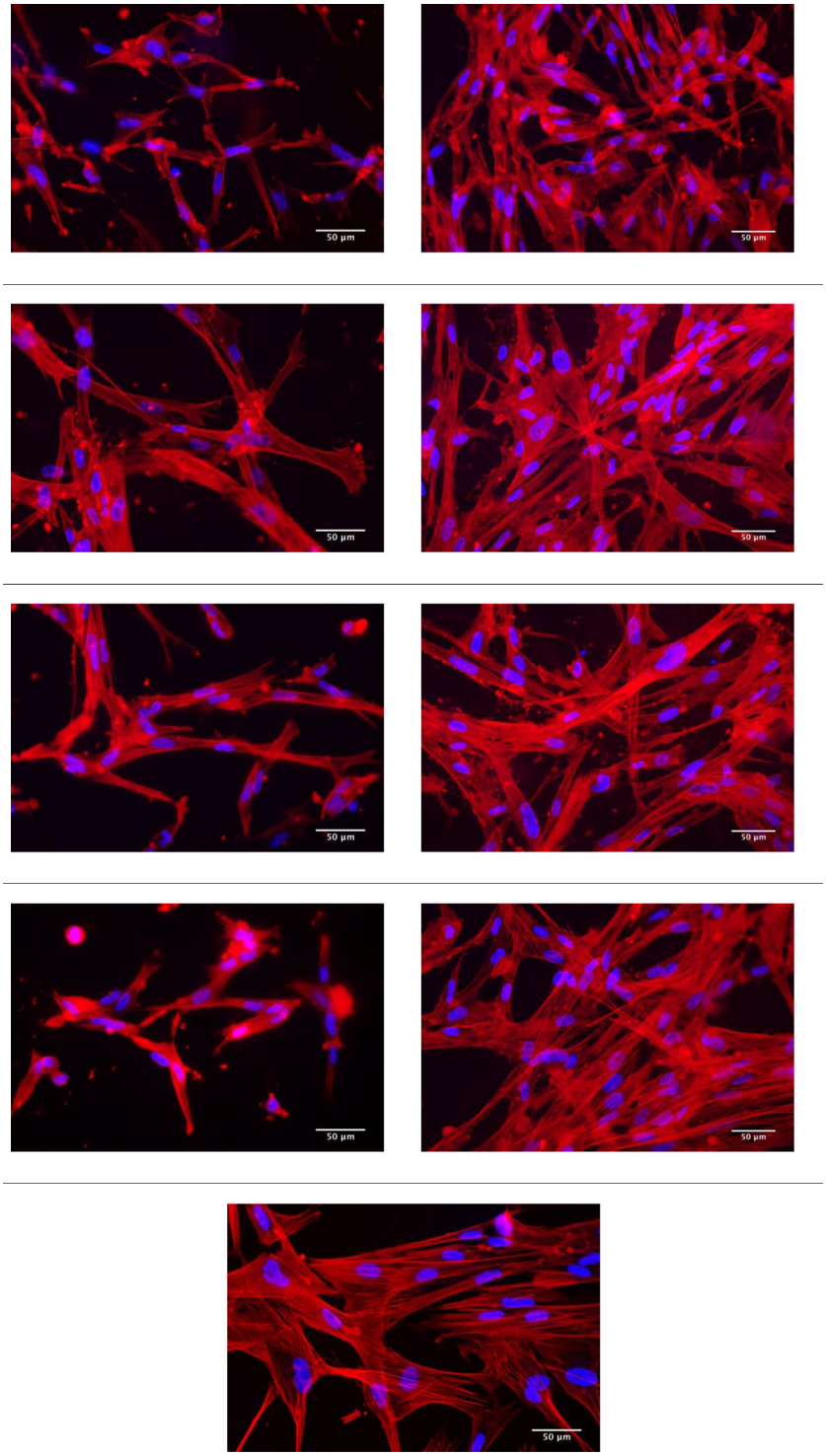

Fig. 6 Fluorescence images of HFFF2 cells grown on the four PCL membranes, fixed with paraformaldehyde and stained with DAPI (blue) and acti-stain 555 phalloidin (red) to reveal the nuclei and F-actin, respectively. First column shows day 2 results, whereas column 2 shows day 10 results. First row: 100:0; second row: 95:5; third row: 90:10; fourth row: 85:15; fifth row: cell control, imaged only on day 2

Conclusions

Results of the present study show that PCL non-woven mats obtained by electrospinning the polymer dissolved in a solvent system consisting of an acetic acid:water mixture containing 5 or 10 wt% of water display the best overall properties as scaffolds for soft Tissue Engineering applications. Additionally, in view of the importance of matching the rates of scaffold degradation and tissue regeneration, adjusting acetic acid:water ratio is an interesting strategy to vary molar mass as a means

of tailoring the resorption rate of PCL scaffolds. This strategy can be applied, with the necessary adaptations regarding the degradation mechanism, to other polymers or even to blends.

Acknowledgements This work was partly funded by FEDER through the COMPETE 2020 Programme and by National funds through FCT – Portuguese Foundation for Science and Technology – under the project UID/CTM/50025/2013.

References

1. Ramakrishna S, Fujihara K, Teo W-E, Lim T-C, Ma Z (2005) An introduction to electrospinning and nanofibers. World Scientific. https://doi.org/10.1142/5894
2. Szentivanyi AL, Zernetsch H, Menzel H, Glasmacher B (2011) A review of developments in electrospinning technology: new opportunities for the design of artificial tissue structures. Int J Artif Organs 34:986–997. https://doi.org/10.5301/ijao.5000062
3. Di Cio S, Gautrot JE (2016) Cell sensing of physical properties at the nanoscale: mechanisms and control of cell adhesion and phenotype. Acta Biomater 30:26–48. https://doi.org/10.1016/j.actbio.2015.11.027
4. Croisier F, Duwez A-S, Jérôme C, Léonard AF, van der Werf KO, Dijkstra PJ, Bennink ML (2012) Mechanical testing of electrospun PCL fibers. Acta Biomater 8:218–224. https://doi.org/10.1016/j.actbio.2011.08.015
5. Chen L, Yan C, Zheng Z (2017) Functional polymer surfaces for controlling cell behaviors. Mater Today 21:38–59. https://doi.org/10.1016/j.mattod.2017.07.002
6. Kim GH (2008) Electrospun PCL nanofibers with anisotropic mechanical properties as a biomedical scaffold. Biomed Mater 3:025010. https://doi.org/10.1088/1748-6041/3/2/025010
7. Gomes SR, Rodrigues G, Martins GG, Roberto M a, Mafra M, Henriques CMR, Silva JC (2015) In vitro and in vivo evaluation of electrospun nanofibers of PCL, chitosan and gelatin: A comparative study. Mater Sci Eng C 46:348–358. https://doi.org/10.1016/j.msec.2014.10.051
8. Cipitria A, Skelton A, Dargaville TR, Dalton PD, Hutmacher DW (2011) Design, fabrication and characterization of PCL electrospun scaffolds—a review. J Mater Chem 21:9419. https://doi.org/10.1039/c0jm04502k
9. Bhaskaran A, Prasad T, Kumary TV, Anil Kumar PR (2018) Simple and efficient approach for improved cytocompatibility and faster degradation of electrospun polycaprolactone fibers. Polym Bull 76:1333–1347. https://doi.org/10.1007/s00289-018-2442-7
10. Thakare VG, Joshi PA, Godse RR, Bhatkar VB, Wadegaokar PA, Omanwar SK (2017) Fabrication of polycaprolactone/zirconia nanofiber scaffolds using electrospinning technique. J Polym Res 24:232. https://doi.org/10.1007/s10965-017-1388-z
11. Kumar AP (2017) Self Organized Skin Equivalent by Epithelial and Fibroblast Cells on Polycaprolactone Electrospun Mat with Porous Fibers. Adv Tissue Eng Regen Med Open Access 3:1–6. https://doi.org/10.15406/atroa.2017.03.00056
12. Jahangiri M, Kalajahi AE, Rezaei M, Bagheri M (2019) Shape memory hydroxypropyl cellulose-g-poly (ε-caprolactone) networks with controlled drug release capabilities. J Polym Res 26:136. https://doi.org/10.1007/s10965-019-1798-1
13. Xie F, Zhang T, Bryant P, Kurusingal V, Colwell JM, Laycock B (2019) Degradation and stabilization of polyurethane elastomers. Prog Polym Sci 90:211–268. https://doi.org/10.1016/j.progpolymsci.2018.12.003
14. Olgun U, Tunç K, Hoş A (2019) Preparation and antibacterial properties of nano biocomposite Poly(ε-caprolactone)-SiO 2 films with nanosilver. J Polym Res 26. https://doi.org/10.1007/s10965-018-1686-0
15. Li WJ, Tuli R, Huang X, Laquerriere P, Tuan RS (2005) Multilineage differentiation of human mesenchymal stem cells in a three-dimensional nanofibrous scaffold. Biomaterials. 26:5158–5166. https://doi.org/10.1016/j.biomaterials.2005.01.002
16. Wise JK, Yarin AL, Megaridis CM, Cho M (2009) Chondrogenic differentiation of human mesenchymal stem cells on oriented nanofibrous scaffolds: engineering the superficial zone of articular cartilage. Tissue Eng Part A 15:913–921. https://doi.org/10.1089/ten.tea.2008.0109
17. Pitt CG, Chasalow FI, Hibionada YM, Klimas DM, Park T, Carolina N (1981) Aliphatic Polyesters . I . The Degradation of Poly (e- caprolactone) In Vivo. J Appl Polym Sci 26:3779–3787. https://doi.org/10.1002/app.1981.070261124
18. Woodward SC, Brewer PS, Moatamed F, Schindler A, Pitt CG (1985) The intracellular degradation of poly(epsilon-caprolactone). J Biomed Mater Res 19:437–444. https://doi.org/10.1002/jbm.820190408
19. Henriques C, Vidinha R, Botequim D, Borges JP, Silva JAMC (2009) A Systematic Study of Solution and Processing Parameters on Nanofiber Morphology Using a New Electrospinning Apparatus. J Nanosci Nanotechnol 9:3535–3545. https://doi.org/10.1166/jnn.2009.NS27
20. Guarino V, Cirillo V, Taddei P, Alvarez-Perez MA, Ambrosio L (2011) Tuning size scale and crystallinity of PCL electrospun fibres via solvent permittivity to address hMSC response. Macromol Biosci 11:1694–1705. https://doi.org/10.1002/mabi.201100204
21. Qin X, Wu D (2012) Effect of different solvents on poly(caprolactone) (PCL) electrospun nonwoven membranes. J Therm Anal Calorim 107:1007–1013. https://doi.org/10.1007/s10973-011-1640-4
22. Van Der Schueren L, De Schoenmaker B, Kalaoglu ÖI, De Clerck K (2011) An alternative solvent system for the steady state electrospinning of polycaprolactone. Eur Polym J 47:1256–1263. https://doi.org/10.1016/j.eurpolymj.2011.02.025
23. Ferreira JL, Gomes S, Henriques C, Borges JP, Silva JC (2014) Electrospinning polycaprolactone dissolved in glacial acetic acid: Fiber production, nonwoven characterization, and in vitro evaluation. J Appl Polym Sci 131:41068. https://doi.org/10.1002/app.41068
24. Li W, Shi L, Zhang X, Liu K, Ullah I, Cheng P (2018) Electrospinning of polycaprolactone nanofibers using H2O as benign additive in polycaprolactone/glacial acetic acid solution. J Appl Polym Sci 135:1–9. https://doi.org/10.1002/app.45578
25. Semnani D, Naghashzargar E, Hadjianfar M, Dehghan Manshadi F, Mohammadi S, Karbasi S, Effaty F (2017) Evaluation of PCL/chitosan electrospun nanofibers for liver tissue engineering. Int J Polym Mater Polym Biomater 66:149–157. https://doi.org/10.1080/00914037.2016.1190931
26. Kaur S, Rana D, Matsuura T, Sundarrajan S, Ramakrishna S (2012) Preparation and characterization of surface modified electrospun membranes for higher filtration flux. J Memb Sci 390–391:235–242. https://doi.org/10.1016/j.memsci.2011.11.045
27. Engler AJ, Sen S, Sweeney HL, Discher DE (2006) Matrix elasticity directs stem cell lineage specification. Cell. 126:677–689. https://doi.org/10.1016/j.cell.2006.06.044
28. Bauer AJP, Wu Y, Liu J, Li B (2015) Visualizing the inner architecture of poly(ϵ-caprolactone)-based biomaterials and its impact on performance optimization. Macromol Biosci 15:1554–1562. https://doi.org/10.1002/mabi.201500175
29. Wang Y, Rodriguez-Perez M a, Reis RL, Mano JF (2005) Thermal and thermomechanical behaviour of polycaprolactone and starch/polycaprolactone blends for biomedical applications. Macromol Mater Eng 290:792–801. https://doi.org/10.1002/mame.200500003

30. Schneider CA, Rasband WS, Eliceiri KW (2012) NIH image to ImageJ: 25 years of image analysis. Nat Methods 9:671–675. https://doi.org/10.1038/nmeth.2089
31. Álvarez E, Vázquez G, Sánchez-Vilas M, Sanjurjo B, Navaza JM (1997) Surface tension of organic acids + water binary mixtures from 20 °C to 50 °C. J Chem Eng Data 42:957–960. https://doi.org/10.1021/je970025m
32. Shin YM, Hohman MM, Brenner MP, Rutledge GC (2001) Experimental characterization of electrospinning: the electrically forced jet and instabilities. Polymer (Guildf). 42:09955–09967. https://doi.org/10.1016/S0032-3861(01)00540-7
33. Fukushima K, Feijoo JL, Yang MC (2012) Abiotic degradation of poly(DL-lactide), poly(ε-caprolactone) and their blends. Polym Degrad Stab 97:2347–2355. https://doi.org/10.1016/j.polymdegradstab.2012.07.030
34. Gholipour Kanani A, Bahrami SH (2011) Effect of changing solvents on poly(-Caprolactone) Nanofibrous webs morphology. J Nanomater 2011:1–10. https://doi.org/10.1155/2011/724153
35. Sajeev US, Anand KA, Menon D, Nair S (2008) Control of nanostructures in PVA, PVA/chitosan blends and PCL through electrospinning. Bull Mater Sci 31:343–351. https://doi.org/10.1007/s12034-008-0054-9
36. Lowery JL, Datta N, Rutledge GC (2010) Effect of fiber diameter, pore size and seeding method on growth of human dermal fibroblasts in electrospun poly(ε-caprolactone) fibrous mats. Biomaterials. 31:491–504. https://doi.org/10.1016/j.biomaterials.2009.09.072
37. Hsu C, Shivkumar S (2004) Nano-sized beads and porous fiber constructs of poly (ε -caprolactone) produced by electrospinning. J Mater Sci 9:3003–3013
38. Wong S-C, Baji A, Leng S (2008) Effect of fiber diameter on tensile properties of electrospun poly(ε-caprolactone). Polymer (Guildf) 49:4713–4722. https://doi.org/10.1016/j.polymer.2008.08.022
39. Johnson J, Niehaus A, Nichols S, Lee D, Koepsel J, Anderson D, Lannutti J (2009) Electrospun PCL in vitro: a microstructural basis for mechanical property changes. J Biomater Sci Polym Ed 20:467–481. https://doi.org/10.1163/156856209X416485
40. Balguid A, Mol A, van Marion MH, Bank R a, Bouten CVC, Baaijens FPT (2009) Tailoring Fiber Diameter in Electrospun Poly(ε-Caprolactone) Scaffolds for Optimal Cellular Infiltration in Cardiovascular Tissue Engineering. Tissue Eng A 15:437–444. https://doi.org/10.1089/ten.tea.2007.0294
41. Tan EPS, Ng SY, Lim CT (2005) Tensile testing of a single ultrafine polymeric fiber. Biomaterials. 26:1453–1456. https://doi.org/10.1016/j.biomaterials.2004.05.021
42. Sun L, Han RPS, Wang J, Lim CT (2008) Modeling the size-dependent elastic properties of polymeric nanofibers. Nanotechnology. 19:455706. https://doi.org/10.1088/0957-4484/19/45/455706
43. Yuan B, Wang J, Han RPS (2015) Capturing tensile size-dependency in polymer nanofiber elasticity. J Mech Behav Biomed Mater 42:26–31. https://doi.org/10.1016/j.jmbbm.2014.11.003
44. Lim CT, Tan EPS, Ng SY (2008) Effects of crystalline morphology on the tensile properties of electrospun polymer nanofibers. Appl Phys Lett 92:141908. https://doi.org/10.1063/1.2857478
45. Silver FH, Freeman JW, DeVore D (2001) Viscoelastic properties of human skin and processed dermis. Skin Res Technol 7:18–23. https://doi.org/10.1034/j.1600-0846.2001.007001018.x
46. Wu C, Jim TF, Gan Z, Zhao Y, Wang S (2000) A heterogeneous catalytic kinetics for enzymatic biodegradation of poly(ϵ-caprolactone) nanoparticles in aqueous solution. Polymer (Guildf). 41:3593–3597. https://doi.org/10.1016/S0032-3861(99)00586-8
47. Vieira T, Silva JC, Borges JP, Henriques C (2018) Synthesis, electrospinning and in vitro test of a new biodegradable gelatin-based poly(ester urethane urea) for soft tissue engineering. Eur Polym J 103:271–281. https://doi.org/10.1016/j.eurpolymj.2018.04.005
48. Martins AM, Pham QP, Malafaya PB, Sousa R a, Gomes ME, Raphael RM, Kasper FK, Reis RL, Mikos AG (2009) The role of lipase and alpha-amylase in the degradation of starch/poly(epsilon-caprolactone) fiber meshes and the osteogenic differentiation of cultured marrow stromal cells. Tissue Eng A 15:295–305. https://doi.org/10.1089/ten.tea.2008.0025
49. Venugopal JR, Zhang Y, Ramakrishna S (2006) In vitro culture of human dermal fibroblasts on electrospun Polycaprolactone collagen Nanofibrous membrane. Artif Organs 30:440–446. https://doi.org/10.1111/j.1525-1594.2006.00239.x
50. Woo KM, Chen VJ, Ma PX (2003) Nano-fibrous scaffolding architecture selectively enhances protein adsorption contributing to cell attachment. J Biomed Mater Res A 67:531–537. https://doi.org/10.1002/jbm.a.10098
51. Chen F, Lee CN, Teoh SH (2007) Nanofibrous modification on ultra-thin poly(e-caprolactone) membrane via electrospinning. Mater Sci Eng C 27:325–332. https://doi.org/10.1016/j.msec.2006.05.004
52. Washburn NR, Yamada KM, Simon CG, Kennedy SB, Amis EJ (2004) High-throughput investigation of osteoblast response to polymer crystallinity: influence of nanometer-scale roughness on proliferation. Biomaterials. 25:1215–1224. https://doi.org/10.1016/j.biomaterials.2003.08.043